Chemical Science

Accepted Manuscript

This article can be cited before page numbers have been issued, to do this please use: C. Huang, X. Chen, W. Zhang, F. Wang, Y. Tu, J. Li and Z. Wei, *Chem. Sci.*, 2025, DOI: 10.1039/D5SC05140A.

ROYAL SOCIETY OF CHEMISTRY

rsc.li/chemical-science

View Article Online
DOI: 10.1039/D5SC05140A

PdGa nanoalloys loaded on single atomic Co dispersed nitrogen doped carbon for ethanol electrooxidation: improved C1 pathway selectivity and durability

Chengming Huang, Xia Chen, Wenjing Zhang, Fangzheng Wang, Yunchuan Tu,* Jing Li,* and Zidong Wei*

State Key Laboratory of Advanced Chemical Power Sources, School of Chemistry and Chemical Engineering, Chongqing University, 401331 Chongqing, China

Abstract：Direct ethanol fuel cells (DEFCs) are among the most efficient and environmentally friendly energy conversion devices, and the development of ethanol oxidation reaction (EOR) catalysts with high C1 pathway selectivity and electrochemical durability is essential for the commercialization of DEFCs. In this study, we demonstrate that engineering single-atom Co dispersed support is an effective strategy for modulating the electronic structure of supported PdGa alloy nanoparticle catalysts, thereby significantly enhancing EOR performance. In alkaline system, PdGa/Co_{SA}-NC exhibits a C1 path selectivity of 34.3% at 0.8 V_{RHE}, being 2.3 and 7.0 times those of PdGa/NC and commercial Pd/C, respectively. Also in the accelerated durability testing PdGa/Co_{SA}-NC well maintains 74.2% and 35.0 % of the initial activity after 1000 and 2500 cycles respectively. Our theoretical calculations show that PdGa alloy nanoparticles exhibit significantly enhanced electron transfer to the Co_{SA}-NC support compared to their PdGa/NC counterpart, leading to a substantial increase in charge density at the interfacial region of the PdGa/Co_{SA}-NC. The well modified electron structures optimize the adsorption energies of key intermediate species on Pd sites, simultaneously promoting both C-C bond cleavage and *CO oxidation, thus enhancing the C1 pathway selectivity and EOR durability on PdGa/Co_{SA}-NC.

Keywords: Direct ethanol fuel cell; Ethanol oxidation reaction; C1 pathway selectivity; PdGa alloy; Single-atomic Co

View Article Online
DOI: 10.1039/D5SC05140A

1. Introduction

Direct ethanol fuel cells (DEFCs) have been recognized as one of the most promising energy power units for portable and mobile applications due to their high energy density, convenient storage/transportation and environmental friendliness [1-4]. It is generally accepted that the ethanol oxidation reaction (EOR) follows the C1/C2 dual pathway reaction mechanism [5-8]. And the incomplete oxidation of ethanol to acetic acid or acetate products (C2 pathway), with only 4 e^- transfer, leads to the incomplete utilization of ethanol fuel and greatly reduces the energy conversion efficiency. In contrast, the complete oxidation of ethanol to CO_2 (C1 pathway) can maximize the energy release due to the transfer of 12 e^-. However, the high energy barrier of C-C bond cleavage and the slow oxidation of various carbonaceous intermediates such as *CH_x and *CO, severely hinder the kinetics of C1 pathway [9-12]. Therefore, the synthesis of EOR catalysts able to accelerate the C1 pathway process, inhibit C2 process, thus enhance the C1 selectivity is crucial for the practical DEFCs.

Presently, noble metal Pd has been widely recognized as the most active catalyst for EOR in alkaline electrolytes [13-17], and to enhance its catalytic performance, the approach of alloying Pd with a secondary metal has proven to be an effective route [18-20]. In general, the enhanced catalytic properties of Pd alloys can be attributed to two main aspects: the second metal can change the electronic structure of Pd, thus promoting the C-C bond breaking for higher C1 pathway selectivity; On the other hand, the second component in the alloys can accelerate *OH adsorption, which facilitates the removal of *CH_x and *CO species and then improves reaction kinetics and the anti-poisoning capability of the catalyst [21-28]. However, due to the complexity of the EOR process, the acquired C1 pathway selectivity and the overall catalytic performance remain significantly below the anticipated levels. Consequently, there is an urgent need to develop innovative catalyst design strategies to substantially enhance the various metrics of EOR performance. A few recent reports have indicated that the construction of specific external sites can well modify the electronic structure of nanoalloys, and one of the practically effective ways is the adoption of support material containing singly-dispersed atoms [9, 29-33]. However, the research in this specific field is still limited, and the efficacy of such regulation in electrocatalytic EOR has yet to be substantiated.

Herein, we choose metallic PdGa alloy nanoparticles as the major catalytic sites as they well

View Article Online
DOI: 10.1039/D5SC05140A

facilitate the complete electrooxidation of ethanol due to the p-d orbital hybridization effect [34]. Then by loading PdGa alloy nanoparticles on the single Co atom dispersed N-doped carbon (Co_{SA}-NC), we can investigate the enhancing effect of the atomic level support to the catalytic PdGa alloy centers. Interestingly the prepared PdGa/Co_{SA}-NC catalyst achieves highly efficient EOR catalysis in alkaline electrolyte as the mass activity reaches 6.93 A mg_{Pd}^{-1}, being 2.1 and 5.6 times those of PdGa/NC (3.28 A mg_{Pd}^{-1}) and Pd/C (1.24 A mg_{Pd}^{-1}). Also it exhibits a C1 path selectivity of 34.3% at 0.8 V_{RHE}, being 2.3 and 7.0 times those of PdGa/NC and commercial Pd/C, respectively. And in the accelerated durability testing, PdGa/Co_{SA}-NC well maintains 74.2% and 35.0 % of the initial activity after 1000 and 2500 cycles respectively, exceeding the performances of state-of-the-art materials. Density Functional Theory (DFT) calculations show that PdGa alloy nanoparticles exhibit significantly enhanced electron transfer to the Co_{SA}-NC support compared to their PdGa/NC counterpart, leading to a substantial increase in charge density at the interfacial region of the PdGa/Co_{SA}-NC. The well modified electron structures optimize the adsorption energies of key intermediate species on Pd sites, simultaneously promoting both C-C bond cleavage and *CO oxidation on PdGa/Co_{SA}-NC, which not only enhances the C1 pathway selectivity but also confers superior EOR durability through significantly improved CO tolerance. This study demonstrates that engineering single-atom dispersed supports represents an effective strategy for modulating the electronic structure of supported alloy catalysts, thereby significantly enhancing their electrocatalytic performance. The fundamental understanding provides a valuable framework for the rational design of highly efficient catalysts for various crucial electrocatalytic processes.

View Article Online
DOI: 10.1039/D5SC05140A

2. Results and Discussion

2.1 Characterization of catalysts

The synthesis process of PdGa/Co_{SA}-NC is schematically illustrated in Figure 1a and the experimental details are given in Supplementary information. Briefly, the metal-organic framework material Zn/Co-ZIF was firstly prepared by introducing a small amount of metallic Co into ZIF-8 during the assembly of the latter [35-36]. After Pd^{2+} and Ga^{3+} were adsorbed on the surface of Zn/Co-ZIF, the obtained composite was calcinated at 900 °C under H_2/Ar flow to form the final product PdGa/Co_{SA}-NC. During this annealing process, Zn species is evaporated at ~ 700 °C, which promotes Co-N bonding, and formation of the single atomic Co dispersed nitrogen-doped carbon Co_{SA}-NC, as displayed in Figure S1. The transmission electron microscopy (TEM), HAADF-STEM and EDX mapping images of PdGa/Co_{SA}-NC (Figure 1b-i and S2) show that PdGa alloy particles possess quite narrow size distribution of 14.0 nm, which together with singly dispersed Co atoms are evenly anchored on the NC support. To illustrate the role of atomic Co, we also prepared a Co-free control sample PdGa/NC by a similar method, except no Co precursor is used (Figure S3). Table S1 gives the composition of the two materials measured by Inductively Coupled Plasma Optical Emission Spectrometer (ICP-OES) which shows that PdGa/Co_{SA}-NC and PdGa/NC own quite similar Pd content of 3.9 wt% and Ga content of 3.4 wt%, and Zn species is almost non-existent in both.

View Article Online
DOI: 10.1039/D5SC05140A

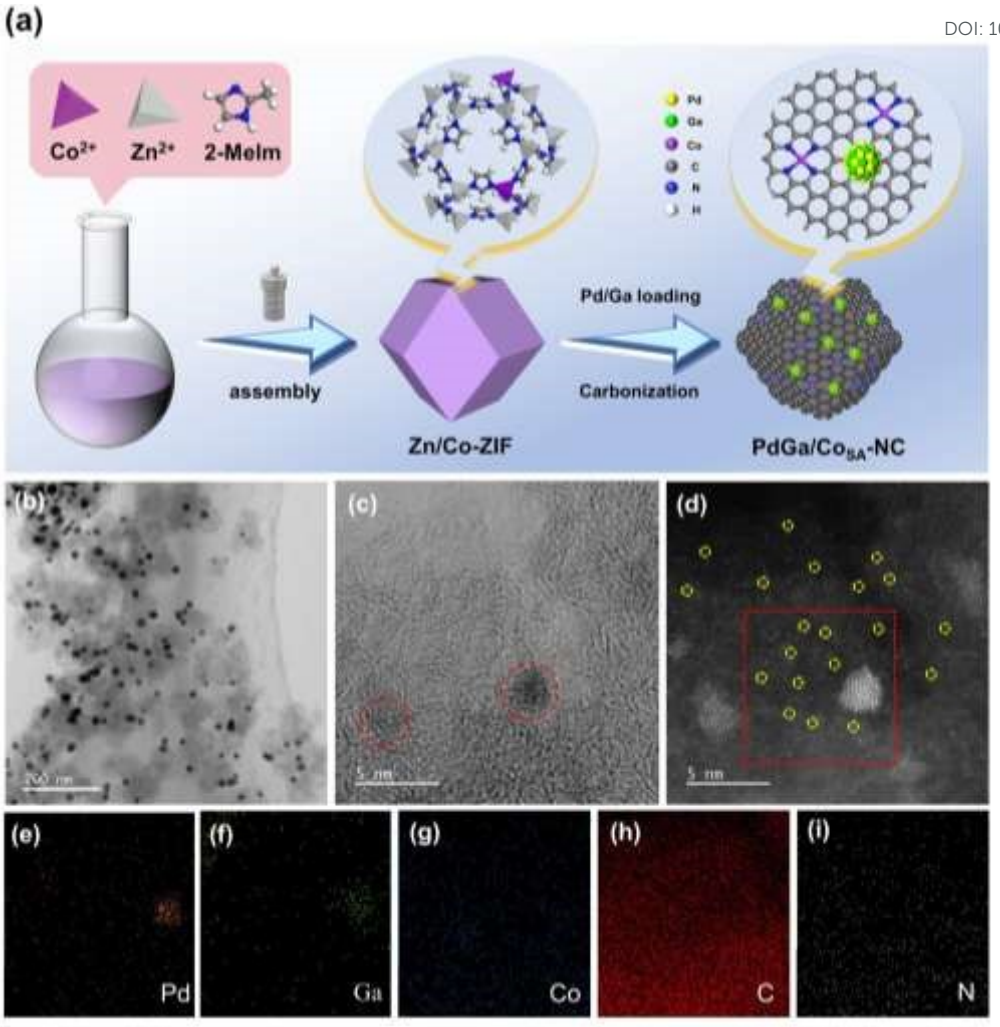

Figure 1. Synthesis and characterization of PdGa/Co_{SA}-NC. (a) Schematic illustration of the synthetic process for PdGa/Co_{SA}-NC; (b, c) TEM images of PdGa/Co_{SA}-NC; (d-i) HAADF-TEM image and corresponding elemental maps of PdGa/Co_{SA}-NC.

Figure 2a shows the X-ray diffraction (XRD) patterns. PdGa/Co_{SA}-NC displays two distinct diffraction peaks at 2θ of 41.6° and 46.0°, which compared to (210) and (211) crystal planes of PdGa alloy (No. 50-1442), both shift 1.2° to the higher 2θ direction. Considering the mapping results in Figure 1g shows that Co signal does not raise in the PdGa alloy position, the alloy composition is determined to be PdGa instead of PdGaCo, and the peak shift might be due to the lattice shrinkage induced by the strong interaction between alloy particles and the Co_{SA}-NC support [37-38]. As listed in Table S2, the lattice parameters of PdGa/Co_{SA}–NC and PdGa/NC catalysts are compared [39-40]. The results indicate that, relative to the NC support, the formation of the Co_{SA}–NC support induces

View Article Online
DOI: 10.1039/D5SC05140A

a compressive lattice strain of 0.69% in the PdGa alloy. Besides, no metallic cobalt peaks were detected, confirming the absence of cobalt nanoparticle formation, which is primarily attributed to the low Co:Zn atomic ratio (1:99) in the precursors. In comparison, PdGa/NC gives multiple diffraction peaks, and the two located at 41.4° and 44.7° match well with those of PdGa. Besides, the peak located at 41.4°, as well as the two located at 39.7° and 35.8°, can be well attributed to the (013), (210), and (112) crystal plane of Pd_2Ga alloy (No. 50-1443). This observation exhibits that there has a mixed phase of PdGa and Pd_2Ga in PdGa/NC. This conclusion is further validated by Selected Area Electron Diffraction (SAED) analysis, as shown in Figure S4. For PdGa/Co_{SA}-NC, diffraction patterns corresponding to the (210) and (211) planes of the PdGa alloy were observed. In contrast, PdGa/NC exhibited diffraction patterns from (210) and (211) planes of the PdGa alloy, as well as (112) and (211) planes of the Pd_2Ga alloy. Particularly, the single phase PdGa formed on Co_{SA}-NC and the mixed PdGa/Pd_2Ga phase acquired on NC inspire our interest to investigate if the single atomic Co in the NC support could affect the alloy composition. Using DFT method, we calculated the formation energies of $PdGa_2$, PdGa, and Pd_2Ga alloy particles on Co_{SA}-NC and NC supports respectively (Figure S5-6, Supporting Information). As displayed in Figure 2b, on Co_{SA}-NC, the formation energies of $PdGa_2$ (-0.70 eV) and Pd_2Ga (-0.52 eV) are greatly higher than that of PdGa (-1.90 eV), and on NC, the formation energies of PdGa (-1.62 eV) and Pd_2Ga (-1.82 eV) are significantly lower than that of $PdGa_2$ (-0.30 eV), which well indicates that Co_{SA}-NC surface favors formation of single phase PdGa particles while NC is more prone to acquiring mixed PdGa/Pd_2Ga phase, being in good agreement with above XRD results.

View Article Online
DOI: 10.1039/D5SC05140A

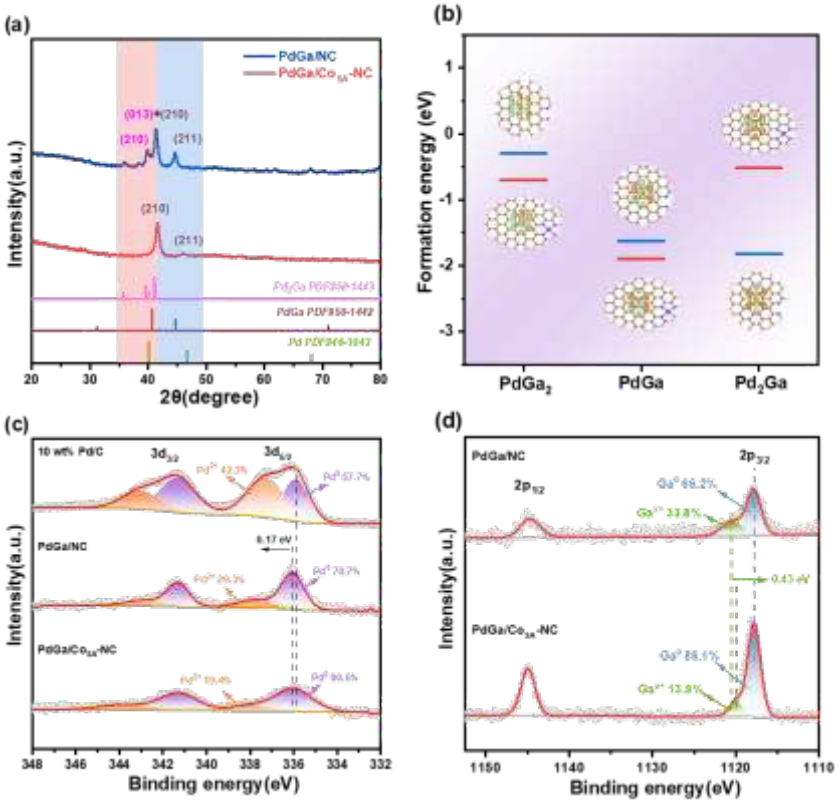

Figure 2. Structural characterization of the as-prepared catalysts. (a) XRD patterns; (b) Formation energies of $PdGa_2$, PdGa and Pd_2Ga on Co_{SA}-N-C or N-C, respectively; (c) Pd 3d XPS spectra; (d) Ga 2p XPS spectra.

X-ray photoelectron spectroscopy (XPS) tests were used to investigate the chemical composition and elemental valence states. As shown in Figure 2c-d, the contents of Pd^0 and Ga^0 in PdGa/Co_{SA}-NC reach 80.6% and 86.1% respectively, being significantly higher than the corresponding values of 70.7% and 66.2% in PdGa/NC. Considering that metallic species are typically more active in electrocatalysis, this observation may imply a higher activity of PdGa/Co_{SA}-NC than PdGa/NC [41-42]. In addition, the high resolution XPS spectra of Co 2p (Figure S7, Supporting Information) show that PdGa/Co_{SA}-NC contains only Co^{2+} and no Co^0 and Co^{3+}, and simultaneously Co-N species has been detected in the N 1s spectra. It clearly demonstrates the formation of Co – N coordination by which elemental Co mainly exists in the form of single atoms in PdGa/Co_{SA}-NC [42-43].

2.2 Electrocatalytic tests in EOR

The electrocatalytic EOR performances of commercial Pd/C, PdGa/NC and PdGa/Co_{SA}-NC catalysts were evaluated using standard three-electrode tests conducted in N_2-saturated 1 M KOH + 1 M CH_3CH_2OH electrolyte (Figure 3a-d and S8-9). In our work, the onset potential was identified as the potential where the current density measured in KOH + EtOH begins to exceed that in KOH alone, as determined from the CV curves in Figure S8. Linear sweep voltammetry (LSV) polarization curves collected at a scan rate of 10 mV s^{-1} show that the onset EOR potential occurred on PdGa/Co_{SA}-NC is only 0.20 V, which is negatively shifted by 40 and 100 mV compared to those of PdGa/NC (0.24 V) and Pd/C (0.30 V) respectively, indicating more readily EOR on PdGa/Co_{SA}-NC. CO stripping voltammetry shows that the CO onset oxidation potential on PdGa/Co_{SA}-NC is 20 and 70 mV lower than those on PdGa/NC and Pd/C respectively, representing that PdGa/Co_{SA}-NC has better anti-CO poisoning capability [44-45]. The estimated electrochemical active surface area (ECSA) is 54.76 $m^2\ g_{Pd}^{-1}$ for PdGa/Co_{SA}-NC, which is also higher than those of PdGa/NC (45.81 $m^2\ g_{Pd}^{-1}$) and Pd/C (41.35 $m^2\ g_{Pd}^{-1}$). Particularly, the mass activity of PdGa/Co_{SA}-NC reaches 6.93 A mg_{Pd}^{-1}, which is 2.1 and 5.6 times those of PdGa/NC (3.28 A mg_{Pd}^{-1}) and Pd/C (1.24 A mg_{Pd}^{-1}) respectively, and the specific activities follow the same trend. Additionally, the catalytic kinetics were further evaluated through Tafel slope and Electrochemical impedance spectroscopy (EIS) (Figure S10). PdGa/Co_{SA}-NC exhibited the lowest Tafel slope (178 mV dec^{-1}) and the smallest charge transfer resistance (30.0 Ω), indicating superior performance over both PdGa/NC and commercial Pd/C. These results suggest enhanced catalytic activity and improved reaction kinetics for the PdGa/Co_{SA}-NC catalyst [46-47]. We also compared the mass activity with the top ones reported recently in Table S3, in which our catalyst is quite excellent.

View Article Online
DOI: 10.1039/D5SC05140A

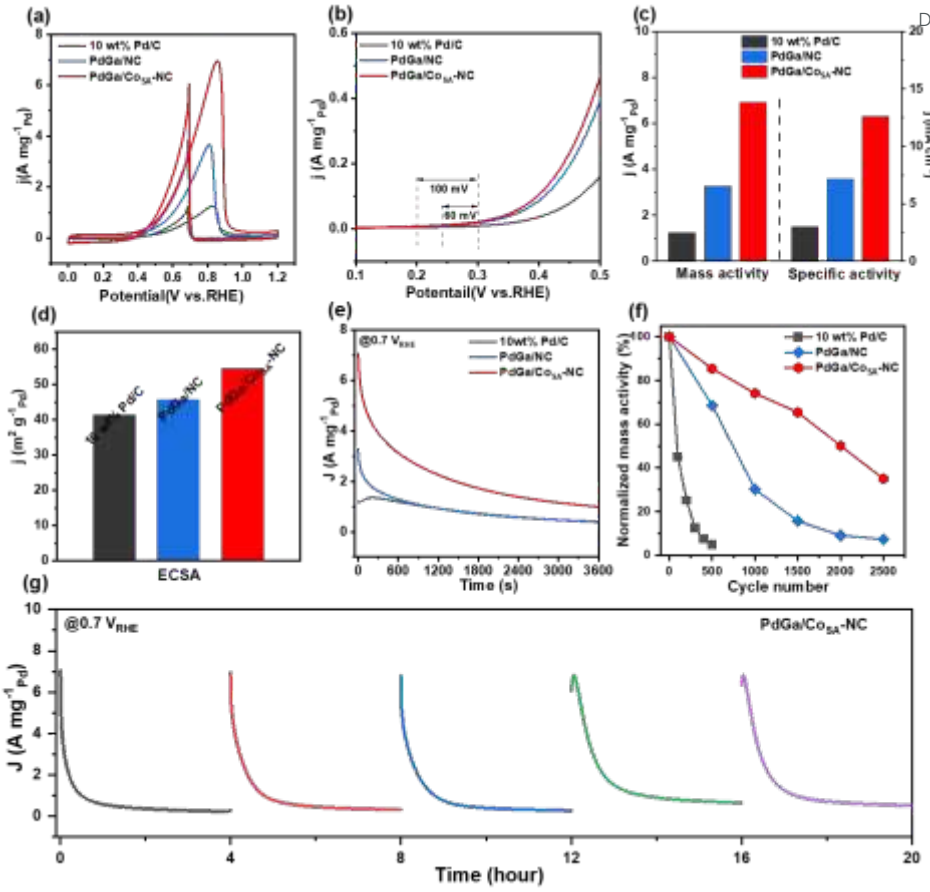

Figure 3. Catalyst EOR performance measurements. (a) Mass-normalized CV curves, (b) Mass-normalized LSV curves, (c) MA and SA, (d) ECSA, (e) CA curves at 0.7 V_{RHE}, (f) ADT tests of PdGa/Co$_{SA}$-NC, PdGa/NC and commercial Pd/C in 1 M KOH + 1 M C_2H_5OH; (g) Long-term durability of PdGa/Co$_{SA}$-NC. The catalyst reactivation and electrolyte replacement after every 4 hour.

EOR durability of PdGa/Co$_{SA}$-NC was studied by three methods. Firstly, in the chronoamperometry (CA) tests, the current-time (i-t) curves (Figure 3e) were recorded under a constant voltage of 0.7 V for 3600 s in N_2-saturated 1 M KOH + 1 M CH_3CH_2OH electrolyte. PdGa/Co$_{SA}$-NC gives continuously higher current density with the slower current decrease rate than the other two catalysts throughout the test range. Secondly, we cycled the CA tests for 5 times by replacing the used electrolyte with fresh one every 4 hour. Figure 3g and S11 show that PdGa/Co$_{SA}$-NC well remains the initial activity along this process, whereas PdGa/NC and Pd/C gradually deteriorate along increased cycle number, and their 5th cycles provide only 39 % and 18 % of the initial current density respectively. Thirdly, the accelerated durability testing (ADT) was conducted

by applying multiple CV cycling in N_2-saturated 1 M KOH+1 M CH_3CH_2OH solution. As shown in Figure 3f and S12, Pd/C deactivates almost completely (only 4.8 % activity remained) after 500 cycles. PdGa/NC is able to maintain 30.2 % of the initial activity after 1000 cycles, while after 1500 cycles, the remained activity is not more than 20.0%. In comparison, PdGa/Co_{SA}-NC well maintains 85.5% and 74.2% of the initial activity after 500 and 1000 cycles respectively, and after 2500 consecutive cycles, there still has 35.1% activity left. We then investigated the microscopic morphology evolution of the PdGa/Co_{SA}-NC catalysts. As shown in Figure S13, following the ADT, PdGa nanocrystals in the PdGa/Co_{SA}-NC catalyst exhibited only a slight size increase from 14.0 nm to 14.8 nm, and the single-atomic dispersion of Co sites remained unchanged. Therefore, the excellent structural stability, combined with high CO poisoning resistance, accounts for the outstanding durability of the PdGa/Co_{SA}-NC catalyst. All above observations clarify the superior activity and durability of PdGa/Co_{SA}-NC in electrocatalytic EOR, and the intrinsic mechanism was further investigated by *in-situ* FTIR spectra and DFT methods.

2.3 Reaction mechanism

Electrochemical *in-situ* FTIR spectra were collected at the potentials ranging from 0.3 to 1.2 V_{RHE} with a spacing of 0.1 V. In Figure 4a-c, the three characteristic peaks located at 1346, 1415 and 1550 cm^{-1} are attributed to the bending vibration of -CH_3, the symmetric and asymmetric stretching bonds of O-C-O in CH_3COO^- respectively, which indicate the formation of C2 products. Interestingly, the three peaks are observed from 0.6 V on Pd/C, 0.5 V on PdGa/NC, and 0.4 V on PdGa/Co_{SA}-NC, revealing the faster EOR kinetics on PdGa/Co_{SA}-NC. Besides, the band of the possible C1 product CO_3^{2-} is located at 1390 cm^{-1}, which is overlapped with the peak at 1415 cm^{-1} assigned to acetate. We then roughly distinguish the presence of CO_3^{2-} by a peak splitting. In Figure S14, the CO_3^{2-} relative spectral peak intensity of PdGa/Co_{SA}-NC is significantly higher than those of Pd/C and PdGa/NC over the full range from 0.6 to 0.9 V_{RHE}, suggesting that PdGa/Co_{SA}-NC catalyst may possess a higher C1-pathway selectivity in the EOR process. To more accurately determine the C1 route selectivity, subtractive spectroscopy was used to exclude the contribution of CH_3COO^- at 1415 cm^{-1}, by which the relative concentrations (C_R) of CH_3COO^- and CO_3^{2-} and the C1-pathway selectivity η have been calculated (Figure 4d and S15) [34, 48-50]. Particularly, η of

PdGa/Co_{SA}-NC is much higher than those of PdGa/NC and Pd/C over the potentials from 0.6 to 1.2 V_{RHE}, implying PdGa/Co_{SA}-NC is very favorable to get complete oxidation of ethanol. In addition, the oxidation products after long-term CA tests at different potentials were quantitatively analyzed by ^{1}H NMR using the external standard curve method (Figure S16 and S17), by which we further calculate the Faraday efficiencies (FEs). Figure 4e shows that FEs of PdGa/Co_{SA}-NC for C1 pathway are consistently better than those of PdGa/NC and Pd/C. The highest C1 selectivity on PdGa/Co_{SA}-NC was acquired at the applied potential of 0.8 V_{RHE}, which reaches 34.3%, being much higher than the corresponding values achieved on PdGa/NC (15.1%) and Pd/C (4.9%). The electrochemical test results and the *in-situ* FTIR analyses suggest that PdGa/Co_{SA}-NC in EOR delivers the higher activity, durability and C1-pathway selectivity compared to PdGa/NC. It was deduced that the single atomic Co_{SA}-NC support may play an essential role for which we further conducted a DFT calculation study.

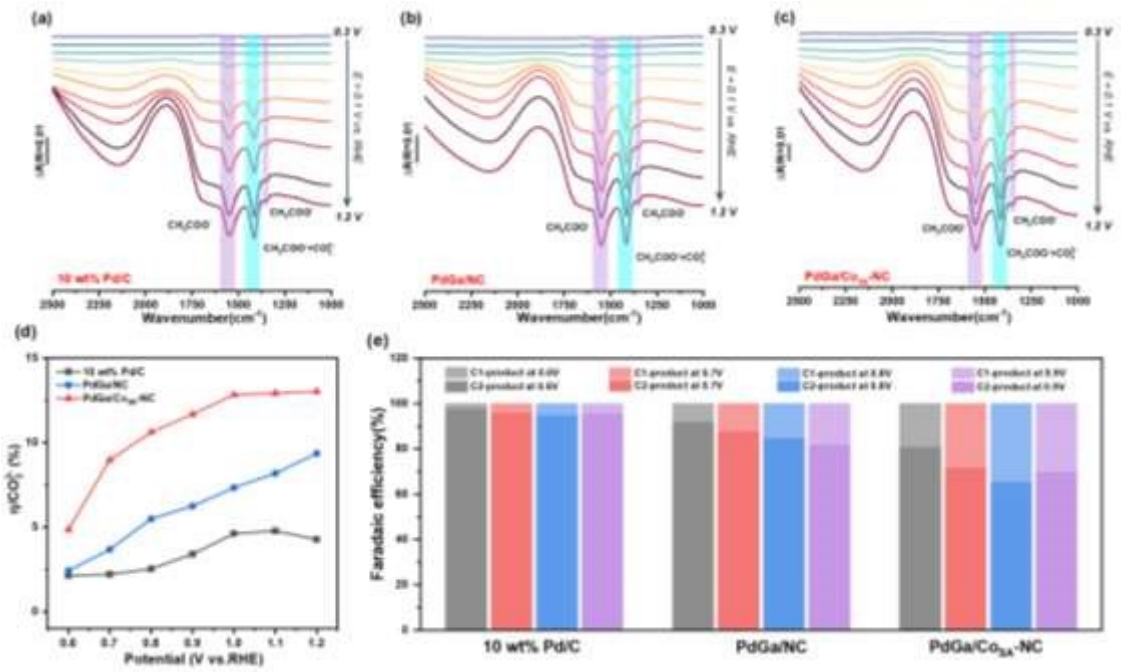

Figure 4. Electrochemical in situ FTIR spectra of (a) commercial Pd/C, (b) PdGa/NC and (c) PdGa/Co_{SA}-NC in 1 M KOH + 1 M C_2H_5OH; (d) The selectivity (η) for complete ethanol oxidation to CO_3^{2-} from 0.6 to 1.2 V_{RHE}; (e) The Faradaic efficiencies of C1 pathway and C2 pathway from 0.6 to 0.9 V_{RHE} of catalysts.

In our DFT calculations, two structures, the PdGa alloys with atomic Pd:Ga ratio of 1:1 were constructed on Co_{SA}-NC and NC substrates respectively (Figure 5a). Then the free energy diagrams along C1 and C2 EOR pathways were investigated (Figure 5b-c, S18). For C1-12e pathway, the C-C bond splitting of $*CH_3CO \rightarrow *CO$ exhibits a lower energy barrier on PdGa/Co_{SA}-NC (0.07 eV) than that on PdGa/NC (0.12 eV), suggesting that PdGa/Co_{SA}-NC has a higher C1 pathway selectivity. Besides, the rate determining step (RDS) of C1 path is combination of *CO and *OH to produce *COOH, and its barrier of 0.48 eV on PdGa/Co_{SA}-NC is distinctly lower than the value of 0.81 eV on PdGa/NC [51-53]. This implies that PdGa/Co_{SA}-NC is more favorable to C1 pathway and is also better resistant to CO poisoning than PdGa/NC. In C2 route, the RDS is $*CH_3CO$ oxidation to $*CH_3COOH$, which exhibits a higher barrier on PdGa/Co_{SA}-NC (0.73 eV) than on PdGa/NC (0.38 eV), implying that C2 pathway occurs less frequently on PdGa/Co_{SA}-NC.

The above observation clarifies that PdGa/Co_{SA}-NC is more favorable to C1 pathway and less favorable to C2 pathway, and the opposite is true for PdGa/NC. We thus consider the single atom Co dispersed Co_{SA}-NC support in the former may play an important role, and give it a deeper discussion. Bader charge analysis indicates that in PdGa/Co_{SA}-NC, PdGa alloy transfers 0.33 e^- to Co_{SA}-NC support, being more than the corresponding value of 0.25 e^- occurred in PdGa/NC. The planar-averaged charge density difference (CDD) plots (Figure 5d-e) show that for both catalysts, a distinct peak appears at the interface of PdGa alloy and the substrate, implying a substantial charge redistribution at this region. And compared to the charge density of $0.15*10^{-3}$ e/A^3 for PdGa/NC, PdGa/Co_{SA}-NC has a larger value of $0.18*10^{-3}$ e/A^3. This observation matches well with the Bader charge calculation result that more electron transfers on PdGa/Co_{SA}-NC, and both results reveal stronger interface interaction, thus more stable anchoring of PdGa nanoparticles on Co_{SA}-NC than on NC support [54-55]. In addition, such electron interaction further leads to an upward shift of d-band center of PdGa alloy from -1.91 eV for PdGa/NC to -1.38 eV for PdGa/Co_{SA}-NC (Figure 5f). This shows that the transfer of electrons from the PdGa d-orbitals to the adsorbed species is faster because the d-band center is closer to the Fermi energy level [21, 23]. Besides, we also calculated the adsorption energies of $*CH_3CH_2OH$, *OH and *CO, three key species that could greatly affect the EOR pathway, and they all displayed significantly stronger adsorption on PdGa/Co_{SA}-NC compared to PdGa/NC (Figure 5g-h, S19). Therefore for PdGa/Co_{SA}-NC, due to existence of the

View Article Online
DOI: 10.1039/D5SC05140A

single atom Co in the NC support, the adsorption energies of the intermediate species are well optimized which accelerates the C-C bond breaking and *CO oxidation, and simultaneously inhibiting the *CH_3CO oxidation, thus leading to higher C1 pathway selectivity. In addition, the charge transfer between PdGa alloy particles and Co single atoms greatly enhances the interfacial interaction force, and improves the anchoring strength of PdGa alloys on the support, thus significantly boosting the structural stability of PdGa/Co_{SA}-NC. This, coupled with its high resistance to CO poisoning, results in superior electrochemical EOR durability.

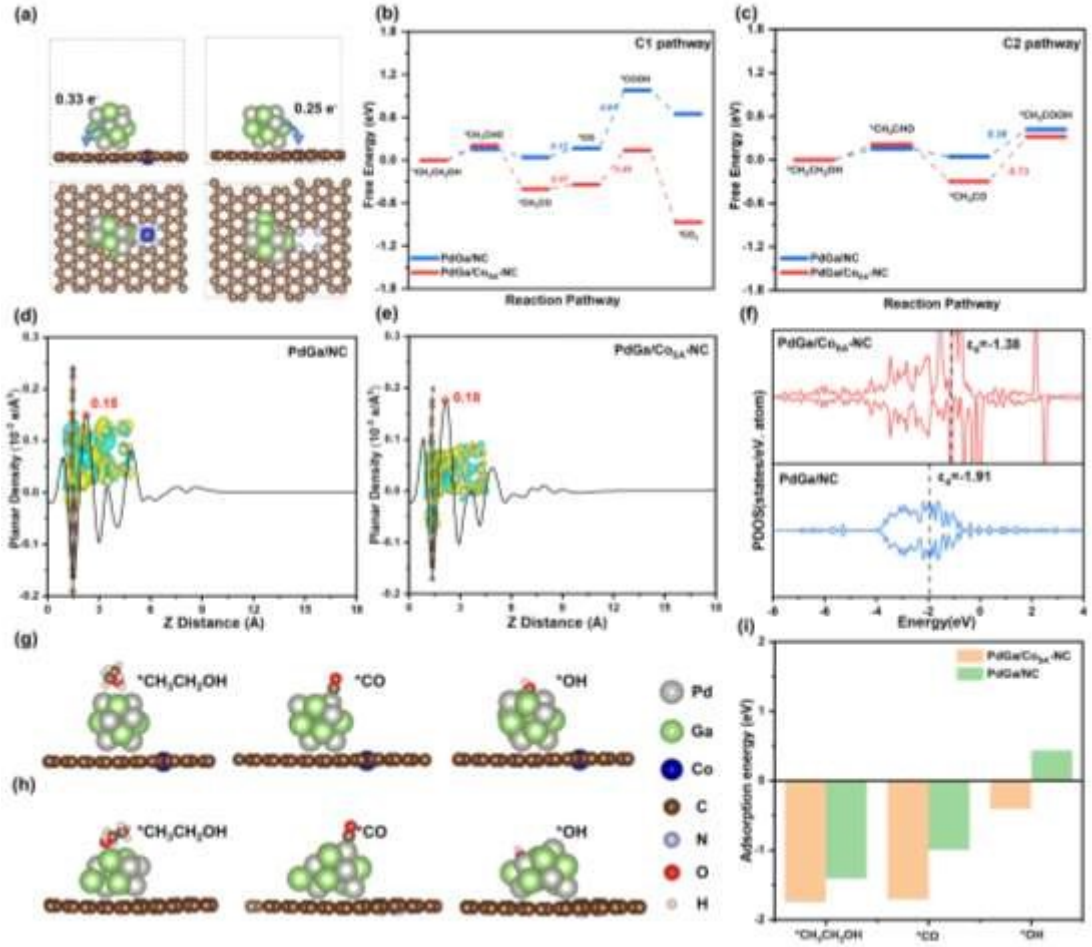

Figure 5. Theoretical calculation. (a) Optimized structures PdGa/Co_{SA}-NC and PdGa/NC (Slide view and top view); (b) Free energy diagram of C1 reaction pathway on PdGa/Co_{SA}-NC and PdGa/NC; (c) Free energy diagram of C2 reaction pathway on PdGa/Co_{SA}-NC and PdGa/NC. (d-e) Planar-averaged charge density difference (CDD) of PdGa/Co_{SA}-NC and PdGa/NC. The insets are side views of CDD of PdGa/Co_{SA}-NC and PdGa/NC; (f) The PDOS plots of PdGa/Co_{SA}-NC and PdGa/NC; (g-h) Adsorption configurations of key intermediates on PdGa/Co_{SA}-NC and

View Article Online
DOI: 10.1039/D5SC05140A

PdGa/NC (Slide view); (i) Calculated adsorption energies of *CH_3CH_2OH, *CO and *OH on the surface of PdGa/Co_{SA}-NC and PdGa/NC.

3. Conclusion

In summary, we synthesized a PdGa/Co_{SA}-NC catalyst and demonstrated that engineering single atom Co dispersed support is an effective strategy for boosting the EOR performance of catalytic PdGa alloy centers. In electrochemical EOR, PdGa/Co_{SA}-NC achieves a mass activity of 6.93 A mg_{Pd}^{-1} and a C1 path selectivity of 34.3% at 0.8 V_{RHE}, which are 2.1 and 2.3 times those of the Co-free PdGa/NC counterpart, respectively. Additionally, it exhibited excellent long-term durability, maintaining 74.2% and 35.0% of its initial activity after 1000 and 2500 cycles, respectively. DFT calculations reveal that PdGa alloy nanoparticles exhibit significantly enhanced electron transfer to the Co_{SA}-NC support when compared to PdGa/NC, leading to a substantial increase in charge density at the interfacial region of PdGa/Co_{SA}-NC. This charge redistribution further optimizes the adsorption energies of key intermediate species on Pd sites, promoting C-C bond cleavage and *CO oxidation for enhanced C1 selectivity as well as superior durability. This study offers valuable insights for the rational design of highly efficient catalysts for a range of crucial electrocatalytic processes.

Conflicts of interest

The authors declare no competing financial interest.

Data availability

The data that support the findings of this study are available in the paper and ESI.

Corresponding Authors

Yunchuan Tu − State Key Laboratory of Advanced Chemical Power Sources, School of Chemistry and Chemical Engineering, Chongqing University, 401331 Chongqing, China; Email: yctu@cqu.edu.cn

View Article Online
DOI: 10.1039/D5SC05140A

Jing Li − State Key Laboratory of Advanced Chemical Power Sources, School of Chemistry and Chemical Engineering, Chongqing University, 401331 Chongqing, China; Email: lijing@cqu.edu.cn

Zidong Wei − State Key Laboratory of Advanced Chemical Power Sources, School of Chemistry and Chemical Engineering, Chongqing University, 401331 Chongqing, China; Email: zdwei@cqu.edu.cn

Authors

Chengming Huang − State Key Laboratory of Advanced Chemical Power Sources, School of Chemistry and Chemical Engineering, Chongqing University, 401331 Chongqing, China

Xia Chen − State Key Laboratory of Advanced Chemical Power Sources, School of Chemistry and Chemical Engineering, Chongqing University, 401331 Chongqing, China

Wenjing Zhang − State Key Laboratory of Advanced Chemical Power Sources, School of Chemistry and Chemical Engineering, Chongqing University, 401331 Chongqing, China

Fangzheng Wang − State Key Laboratory of Advanced Chemical Power Sources, School of Chemistry and Chemical Engineering, Chongqing University, 401331 Chongqing, China

Acknowledgements

This work was financially supported by the National Key Research and Development Program of China (2022YFA1504200), and the National Natural Science Foundation of China (Grant No. 22279012).

References

[1] Z. Meng, Z. Qiu, Y. Shi, S. Wang, G. Zhang, Y. Pi and H. Pang, *Escience*, 2023, **3**, 100092.

[2] M. K. Debe, *Nature*, 2012, **486**, 43-51.

[3] M. Li, D. A. Cullen, K. Sasaki, N. S. Marinkovic, K. More and R. R. Adzic, *J. Am. Chem. Soc.*, 2013, **135**, 132-141.

View Article Online
DOI: 10.1039/D5SC05140A

[4] X. Fu, C. Wan, Y. Huang and X. Duan, *Adv. Funct. Mater*., 2022, **32**, 2106401.

[5] H. Wang and Z. Liu, *J. Am. Chem. Soc.*, 2008, **130**, 10996-11004

[6] Y. Zhu, L. Bu, Q. Shao and X. Huang, *ACS Catal.*, 2019, **9**, 6607-6612.

[7] S. Bai, Y. Xu, K. Cao and X. Huang, *Adv. Mater.*, 2021, **33**, 2005767.

[8] B. Lan, Q. Wang, Z. Ma, Y. Wu, X. Jiang, W. Jia, C. Zhou and Y. Yang, *Appl. Catal. B-Environ.*, 2022, **300**, 120728.

[9] Y. Wang, M. Zheng, Y. Li, C. Ye, J. Chen, J. Ye, Q. Zhang, J. Li, Z. Zhou, X. Fu, J. Wang, S. Sun and D. Wang, *Angew. Chem. Int. Ed*., 2022, **134**, 202115735.

[10] X. Yuan, Y. Zhang, M. Cao, T. Zhou, X. Jiang, J. Chen, F. Lyu, Y. Xu, J. Luo, Q. Zhang and Y. Yin, *Nano Lett.*, 2019, **19**, 4752-4759.

[11] W. Huang, X. Ma, H. Wang, R. Feng, J. Zhou, P. N. Duchesne, P. Zhang, F. Chen, N. Han, F. Zhao, J. Zhou, W. Cai and Y. Li, *Adv. Mater.*, 2017, **29**, 1703057.

[12] Z. Zhang, Q. Wu, K. Mao, Y. Chen, L. Du, Y. Bu, O. Zhuo, L. Yang, X. Wang and Z. Hu, *ACS Catal.*, 2018, **8**, 8477-8483.

[13] C. Liang, R. Zhao, T. Chen, Y. Luo, J. Hu, P. Qi and W. Ding, *Adv. Sci.*, 2024, **11**, 2308958.

[14] H. Fu, Z. Chen, X. Chen, F. Jing, H. Yu, D. Chen, B. Yu, Y. Hu and Y. Jin, *Adv. Sci.*, 2024, **11**, 2306132.

[15] T. Wu, J. Fan, Q. Li, P. Shi Q. Xu and Y. Min, *Adv. Energy Mater.*, 2018, **8**, 1701799.

[16] Y. Fang, S. Guo, D. Cao, G. Zhang, Q. Wang, Y. Chen, P. Cui, S. Cheng and W. Zuo, *Nano Res*., 2022, **15**, 3933-3939.

[17] Y. Wang, M. Li, Z. Yang, W. Lai, J. Ge, M. Shao, Y. Xiang, X. Chen and H. Huang, *Mater. Horiz.*, 2023, **10**, 1416-1424.

[18] H. Xu, H. Shang, C. Wang and Y. Du, *Small*, 2021, **17**, 2005092;

[19] K. Zhang, C. Wang, F. Gao , Si. Guo, Y. Zhang, X. Wang , S. Hata, Y. Shiraishi and Y. Du, *Coordin. Chem. Rev.*, 2022, **472**, 214775.

[20] X. Wu, Y. Wang and Z. Wu, *Chem*, 2022, **8**, 2594-2629.

[21] Y. Qin, H. Huang, W. Yu, H. Zhang, Z. Li, Z. Wang, J. Lai, L. Wang and S. Feng, *Adv. Sci.*, 2022, **9**, 2103722.

[22] H. Lv, L. Sun, Y. Wang, S. Liu and B. Liu, *Adv. Mater.*, 2022, **34**, 2203612.

[23] L. Ji, H. Che, N. Qian, J. Li, S. Luo, X. Li, X. Wu, Q. Xu, X. Gong, X. Cui, H. Zhang and D. Yang, *Appl. Catal. B: Environ.*, 2023, **328**, 122521.

[24] A. P. Chandran, S. Mondal, D. Goud, D. Bagchi, A. K. Singh, M. Riyaz, N. Dutta and S. C. Peter, *Adv. Mater.*, 2025, **37**, 2415362.

[25] Y. Liu, M. Wei, D. Raciti, Y. Wang, P. Hu, J. H. Park, M. Barclay and C. Wang, *ACS Catal.*, 2018, **8**, 10931-10937.

[26] K. Jiang, P. Wang, S. Guo, X. Zhang, X. Shen, G. Lu, D. Su and X. Huang, *Angew. Chem. Int. Edit.*, 2016, **128**, 9176-9181.

[27] P. C. Ashly, S. Sarkar, S. C. Sarma, K. Kaur, U. K. Gautam and S. C. Peter, *J. Power Sources*, 2021, **506**, 230168.

[28] R. Jana, A. Datta and S. Malik, *Chem. Commun.*, 2021, **57**, 4508-4511.

[29] G. Chen, C. Xu, X. Huang, J. Ye, L. Gu, G. Li, Z. Tang, B. Wu, H. Yang, Z. Zhao, Z. Zhou, G. Fu and N. Zheng, *Nat. Mater.*, 2016, **15**, 564-569.

[30] S. Li, A. Guan, H. Wang, Y. Yan, H. Huang, C. Jing, L. Zhang, L. Zhang and G. Zheng, *J. Mater. Chem. A*, 2022, **10**, 6129-6133.

[31] F. Wang, J. Yang, J. Li, Y. Han, A. Li, R. Xu, X. Feng, T. Wang, C. Tong, J. Li and Z. Wei, *ACS Energy Lett.*, 2023, **9**, 93-101.

[32] J. Ruan, Y. Chen, G. Zhao, P. Li, B. Zhang, Y. Jiang, T. Ma, H. Pan, S. Dou and W. Sun, *Small*, 2022, **18**, 2107067.

[33] J. Liu, J. Bak, J. Roh, K. Lee, A. Cho, J. W. Han and E. Cho, *ACS Catal.*, 2020, **11**, 466-475.

[34] G. Zhang, C. Hui, Z. Yang, Q. Wang, S. Cheng, D. Zhang, P. Cui and J. Shui, *Appl. Catal. B: Environ.*, 2024, **342**, 123377.

[35] Z. Wang, C. Zhu, H. Tan, J. Liu, L. Xu, Y. Zhang, Y. Liu, X. Zou, Z. Liu and X. Lu, *Adv. Funct. Mater.*, 2021, **31**, 2104735.

[36] X. Yan, D. Liu, P. Guo, Y. He, X. Wang, Z. Li, H. Pan, D. Sun, F. Fang and R. Wu, *Adv. Mater.*, 2023, **35**, 2210975.

[37] C. L. Tracy, S. Park, D. R. Rittman, S. J. Zinkle, H. Bei, M. Lang, R. C. Ewing and W. L. Mao, *Nat. Commun.*, 2017, **8**, 15634.

[38] K. Sun, W. Mao, L. Jin, W. Shi, W. Niu, C. Wei, Y. He, Q. Yan, R. Wang, Y. Li and B. Zhang,

View Article Online
DOI: 10.1039/D5SC05140A

Angew. Chem. Int. Ed., 2025, **64**, e202502250.

[39] A. Q. K. Nguyen, T. T. Huynh, N. N. Dang and H. Q. Pham, *Chem. Commun.*, 2024, **60**, 14268-14271.

[40] T. T. Huynh, V. T. T. Mai, A. Q. K. Nguyen and H. Q. Pham, *Adv. Sustainable Syst.*, 2024, **8**, 2300380.

[41] H. Liao, C. Wei, J. Wang, A. Fisher, T. Sritharan, Z. Feng and Z. Xu, *Adv. Energy Mater.*, 2017, **7**, 1701129

[42] J. Gao, X. Zhou, Y. Wang, Y. Chen, Z. Xu, Y. Qiu, Q. Yuan, X. Lin and H. Qiu, *Small*, 2022, **18**, 2202071.

[43] Y. He, S. Hwang, D. A. Cullen, M. A. Uddin, L. Langhorst, B. Li, S. Karakalos, A. J. Kropf, E. C. Wegener, J. Sokolowski, M. Chen, D. Myers, D. Su, K. L. More, G. Wang, S. Litster and G. Wu, *Energy Environ. Sci.*, 2019, **12**, 250.

[44] F. Lv, W. Zhang, M. Sun, F. Lin, T. Wu, P. Zhou, W. Yang, P. Gao, B. Huang and S. Guo, *Adv. Energy Mater.*, 2021, **11**, 2100187.

[45] S. Xue, W. Deng, F. Yang, J. Yang, I. S. Amiinu, D. He, H. Tang and S. Mu, *ACS Catal.*, 2018, **8**, 7578.

[46] T. T. Huynh, Q. Huynh, A. Q. K. Nguyen and H. Q. Pham, *Adv. Sustainable Syst.*, 2025, **9**, 2400995.

[47] H. Q. Pham and T. T. Huynh, *J. Phys. Chem. Lett.*, 2023, **14**, 4631−4637.

[48] L. Wang, Z. Yu, W. Yan, L. Liu, M. Wang, Q. Kong, Z. Hu, H. Geng, X. Huang and Y. Li, *Appl. Catal. B: Environ.*, 2024, **343**, 123564.

[49] X. Huang, J. Feng, S. Hu, B. Xu, M. Hao, X. Liu, Y. Wen, D. Su, Y. Ji, Y. Li, Y. Li, Y. Huang, T. Chan, Z. Hu, N. Tian, Q. Shao and X. Huang, *Nat. Nanotechnol.*, 2024, **19**, 1306-1315.

[50] C. Shen, H. Chen, M. Qiu, Y. Shi, W. Yan, Q. Jiang, Y. Jiang and Z. Xie, *J. Mater. Chem. A* 2022, **10**, 1735-1741.

[51] J. Chen, M. Jiang, F. Zhang, L. Wang and J. Yang, *Adv. Mater.*, 2024, **36**, 2401867.

[52] J. Zhu, L. Xia, R. Yu, R. Lu, J. Li, R. He, Y. Wu, W. Zhang, X. Hong, W. Chen, Y. Zhao, L. Zhou, L. Mai and Z. Wang, *J. Am. Chem. Soc.*, 2022, **144**, 15529-15538.

[53] Y. Li, X. Wang, Y. Wang, Z. Shi, Y. Yang, T. Zhao, Z. Jiang, C. Liu, W. Xing and J. Ge, *Carbon*

View Article Online
DOI: 10.1039/D5SC05140A

Energy, 2023, **5**, e310.

[54] W. Li, C. Liu, C. Gu, J. Choi, S. Wang and J. Jiang, *J. Am. Chem. Soc.*, 2023, **145**, 4774-4783.

[55] C. Zhou, J. Shi, Z. Dong, L. Zeng, Y. Chen, Y. Han, L. Li, W. Zhang, Q. Zhang, L. Gu, F. Lv, M. Luo and S. Guo, *Nat. Commun.*, 2024, **15**, 6741.

View Article Online
DOI: 10.1039/D5SC05140A

Data availability

The data that support the findings of this study are available in the paper and ESI.

Conflicts of interest

The authors declare no competing financial interest.